Competitive interactions between Eps15 EH domains and intrinsically disordered proteins generate a complex interaction network

Andromachi Papagiannoula[1#], Ida Marie Vedel[1#], Kathrin Motzny[1], Maud Tengo[2], Sigrid Milles[1,2*]

[1]Leibniz-Forschungsinstitut für Molekulare Pharmakologie, Robert-Rössle-Straße 10, 13125 Berlin, Germany.

[2]Université Grenoble Alpes, CNRS, CEA, IBS, F-38000 Grenoble, France.

[#]equal contribution

*corresponding author, milles@fmp-berlin.de

Abstract

Eps15 is one of the earliest arriving proteins at the endocytic site and is of complex architecture: Its N-terminal domain comprises three small Eps15 homology (EH) domains of less than 10 kDa in size, followed by a coiled coil domain and a C-terminal intrinsically disordered region (IDR) of more than 400 residues in length. The EH domains contribute towards the establishment of a complex interaction network within clathrin mediated endocytosis by interacting with Asp-Pro-Phe (NPF) motifs within intrinsically disordered regions of other endocytic proteins. Using NMR spectroscopy, we investigate the molecular origins of binding from the side of the EH domains as well as from the side of the most intrinsically disordered region of the partner Dab2. In addition to NPF binding, we detect a high level of binding promiscuity leading to significant interaction with non-NPF binding sites. This behavior also leads to interactions between Eps15's EH domains and its own IDR. When all EH domains are expressed in row, as they occur in the wild type full length protein (EH123), EH2 and EH3 tumble together as one entity, while EH1 moves independently. The full EH-domain, comprising EH1, EH2 and EH3, interacts with both Dab2 and Eps15's IDR at the same time with partially competitive binding sites. These data allow insights into competitive network-like interactions determining the early phases of clathrin mediated endocytosis.

Significance Statement

Multi-domain proteins are frequent in many biological processes. Rather than just acting like beads on a string, the EH domains of Eps15 engage in interactions, leading to complex and competitive binding with intrinsically disordered regions (IDRs) involved in Eps15 itself as well as of other endocytic proteins. Such interactions are important to understand how the early phases of clathrin mediated endocytosis are regulated and offer ideas for how interactions may take place in other multi-domain/IDR protein systems. The kind of interactions observed are likely to have implications for liquid-liquid phase separation in endocytosis.

Main Text

Introduction

Clathrin-mediated endocytosis (CME) is the major pathway for cargo uptake into the eukaryotic cell often with transmembrane receptors as cargo. A complex network of interactions are required to take place, which finally leads to the uptake of a clathrin coated vesicle. During the early phases of the process that takes roughly one to two minutes (1), intrinsically disordered protein regions play a major role (2). These disordered regions harbor small interaction regions of often only a few residues (3), also called linear motifs (4) that interact with folded partners, such as the major adaptor protein complex AP2 or clathrin (5–9). Eps15, together with FCHo1/2 proteins, counts among the first proteins to arrive at the endocytic pit (10). It has three N-terminal Eps15 homology domains (EH domains), which share the common fold of two helix-loop-helix motifs (EF-hands) spaced by a short β-sheet (11). The EH domains are followed by a central coiled-coil domain, through which Eps15 dimerizes (12, 13), and then by a large intrinsically disordered region (IDR) of around 400 residues in length (14) (Figure 1F). FCHo1/2 use their C-terminal μ homology domain (μHD) to interact with the Asp-Pro-Phe (DPF) motifs contained in Eps15's IDR (15). The EH domains of Eps15, in turn, bind to Asn-Pro-Phe (NPF) motifs (16) contained in other endocytic proteins, such as Epsin1, Stonin2 (17) or Dab2 (disabled homolog 2) (18). While interactions between EH domains and both Epsin1 and Stonin2 have been characterized at molecular detail, the nature of Dab2's interaction with EH domains remains to date elusive. Dab2 has an N-terminal folded phosphotyrosine interacting domain (PID), which it uses to anchor itself to the membrane and transmembrane cargo, followed by a large IDR of around 500 residues in length, which comprises both DPF as well as NPF motifs (Figure 1A) (19). Both Eps15 and Dab2 belong to the class of clathrin associated sorting proteins (CLASPs), which regulate cargo sorting during the early phases of CME and usually rely on downstream factors, such as the major adaptor protein complex AP2 or clathrin (3, 20, 21). Dab2 has special properties as a CLASP in that it is able to lead to successful CME of specific cargoes even in the absence of AP2. These cargoes are specifically recognized by the Dab2 phosphotyrosine binding (PTB) domain, for example the integrin β1. Importantly, binding of Eps15 to Dab2 is required for the AP2 independent internalization of these protein cargoes (18), highlighting the importance of understanding the communication between Eps15 and Dab2.

Using nuclear magnetic resonance spectroscopy (NMR), we investigate the most disordered region of Dab2, residues 320-495, its conformational sampling, as well as its interactions with all EH domains of Eps15. All EH domains prefer interaction with the only NPF motif within $Dab2_{320\text{-}495}$, but demonstrate a high level of binding promiscuity towards other phenylalanine containing motifs. This is particularly true for the full EH domain, comprising EH1, EH2 and EH3 (EH123), and this promiscuity allows the EH domain to bind to Eps15's own IDR ($Eps15_{IDR}$), which does not possess any NPF motifs – interactions that are possibly involved in liquid-liquid phase separation driving the onset of endocytosis (22). Both, $Dab2_{320\text{-}495}$ and $Eps15_{IDR}$ can bind EH123 simultaneously, but compete with each other in part. This partial competition, allowing the formation of a complex between two IDRs and three folded domains is achieved thanks to the multivalency and binding promiscuity of the different partners and is likely key to a dynamic network that can evolve over time, such as in clathrin mediated endocytosis.

Results

$Dab2_{320-495}$ is an IDR with mild helical propensities.

The around 500 residue long IDR of Dab2 comprises a central region, which is predicted to be significantly more disordered than the remainder of the IDR (Figure 1A). We designed a construct encompassing this region, reaching from residue 320 to 495 ($Dab2_{320-495}$). This region contains 2 putative binding sites for clathrin (DLL/DLF) and one NPF motif, prone to bind to EH domains contained in the CLASP Eps15. We expressed and purified the construct, and assigned the NMR backbone resonances of a ^{1}H, ^{15}N, ^{13}C labeled sample using triple resonance experiments (Figure S1 and S2). We were not able to assign two small regions within $Dab2_{320-495}$, for which we designed two new constructs ($Dab2_{328-360}$ and $Dab2_{358-390}$), whose ^{1}N-^{15}N heteronuclear single quantum coherence (HSQC) spectrum overlaid well with the one of $Dab2_{320-495}$ (Figure S3), enabling the transfer of assignments from $Dab2_{328-360}$ and $Dab2_{358-390}$ to $Dab2_{320-495.}$ As predicted, $Dab2_{320-495}$ appears to be disordered along its entire length, testified by secondary chemical shifts close to zero. However, three regions showed mild helical propensity as compared to random coil: 339-354, 454-460, and 486-490. This is best illustrated by a conformational ensemble calculated on the basis of chemical shifts using a combination of the statistical coil generator flexible meccano (23) and the selection algorithm ASTEROIDS (24). Around the NPF motif, no particular structural propensity could be observed. ^{15}N spin relaxation ($R_{1\rho}$, R_1, $\{^{1}H\}$-^{15}N heteronuclear Overhauser effect - hetNOE) are reminiscent of those of an intrinsically disordered protein. Increased rigidity, testified by increased $R_{1\rho}$ and hetNOE rates is, however, apparent around the transient helix between residues 328 and 360 ($helix_N$), which is connected with the remainder of the disordered chain by a few amino acids of more rapid mobility. The more C-terminal transient helices are also characterized by slightly increased $R_{1\rho}$ and hetNOE rates, appearing, however less pronounced than those of $helix_N$ (Figure S4).

EH1 binds selectively to NPF motifs, while EH2 and EH3 are promiscuous binders.

We then titrated the different Eps15 EH domains (EH1, EH2, or EH3) into ^{15}N $Dab2_{320-495}$ and recorded ^{1}H-^{15}N HSQC spectra at the different titration steps. While small chemical shift perturbations are observed very locally upon addition of EH1, the spectrum of $Dab2_{320-495}$ is more significantly perturbed when EH2 and EH3 are present at comparable concentrations (Figure 1B-E, Figure S5, S6). Plotting the chemical shift perturbations (CSPs) of $Dab2_{320-495}$ upon interaction with the different EH domains along its sequence (Figure 1 C-E) clearly illustrates that EH1, EH2, and EH3 have different binding patterns: EH1 is the most selective of all Eps15 EH domains, binding mainly to the NPF motif of ^{15}N $Dab2_{320-495,}$ while very small CSPs occur around residue 366 only at 200% EH1. EH2 and EH3, on the other hand, were able to interact with multiple small stretches on $Dab2_{320-495}$, revealing a high degree of binding promiscuity. This binding behavior is also mirrored by decreased peak intensities (Figure S6) and increased ^{15}N $Dab2_{320-495}$ $R_{1\rho}$ rates around the respective interaction sites (Figure 2A, B), which reflects the slowed rotational tumbling times of the interacting residues when in contact with the respective EH domains. Residues between the interaction sites have ^{15}N $R_{1\rho}$ rates similar to those of the unbound $Dab2_{320-495}$, suggesting that the different interaction sites act independently from each other. Even though the largest CSPs were observed around the NPF motif also when EH2 and EH3 were added, residues around DYF, WPF, DLF, and DIF motifs were in contact with those

two EH domains at higher EH:Dab2 ratios. Common to all motifs is the Phe residue, suggesting an importance for this residue type in the binding to EH2 and EH3 (Figure 1 C-E). Interestingly, most of these motifs are located in the regions with increased helical propensity of $Dab2_{320-495}$.

The $Dab2_{320-495}$ motifs were furthermore observed to bind to the EH domains with different dynamics. For example, Valine 399, just next to the NPF motif, shows only mild peak broadening upon interaction with EH1, justified by the slowed rotational tumbling times when in complex. Upon interaction with EH2, however, significantly stronger broadening is observed (Figure 2E). The other interacting regions show very little broadening and are mainly characterized by CSPs (Figures 2D). These differential behaviors prompted us to record Carr-Purcell-Meiboom-Gill (CPMG) relaxation dispersion of $Dab2_{320-495}$ to investigate the possibility of intermediate exchange in the microsecond to millisecond regime between the bound and unbound states in the presence of EH2 (Figure 2C). These experiments confirm that the NPF motif binds EH2 in intermediate exchange on the NMR chemical shift timescale. Surprisingly, many residues throughout the transient helix between residues 328-360 ($helix_N$) also displayed dynamics on the intermediate timescale. The remaining motifs were concluded to bind in fast exchange.

In order to quantify the different binding patterns of the EH domains, we attempted to extract dissociation constants (K_D) for the binding with the $Dab2_{320-495}$ interaction motifs. Even though fitting of chemical shift perturbations as a function of EH domain concentration was difficult due to the low affinities and peak broadening (especially around the NPF motif upon interaction of EH2), they can be estimated to be in the high micromolar to millimolar range (Figure S7A). Analysis of the CPMG relaxation dispersion curves of $Dab2_{320-495}$ upon interaction with EH2 revealed a K_D value in a similar range (196 μM), whereby the dispersion in the $helix_N$ and around the NPF motif was fit together (Figure S7B).

Only EH2 uses a second binding pocket.

We wondered whether differences in the EH domains could explain the distinct interactions observed with the different motifs of $Dab2_{320-495}$. We thus set out to study the interactions between $Dab2_{320-495}$ and the Eps15 EH domains from the side of EH1, EH2 and EH3, respectively. Even though NMR assignments of the three EH domains exist (25–27), we assigned all three EH domains under our experimental conditions (Figures S8-S10). From the carbon SCS, we calculated secondary structure propensities (SSP) which are in agreement with previously determined NMR structures of the proteins (Figure S11) (28–30). Additionally, ^{15}N R_1 and $R_{1\rho}$ relaxation rates reflect small folded domains with flexible N- and C-termini as expected (Figure 2F, 3C, S12). We then titrated $Dab2_{320-495}$ into the different ^{15}N labeled EH domains and recorded ^{1}H-^{15}N Transverse relaxation-optimized spectroscopy (TROSY) spectra of the EH domains at the different titration steps (Figure 1G-J). The largest CSPs can be observed around the previously identified binding pockets (17, 29) and are comparable between all three EH domains. A clearly separated binding region, previously shown to bind a second NPF motif in Stonin2 (17), is clearly visible in EH2. The region seems to participate in binding also within EH1 and EH3, albeit in a less pronounced way (Figure 1H-J). $R_{1\rho}$ relaxation rates systematically increase throughout all residues when $Dab2_{320-495}$ is titrated into the ^{15}N labeled EH domains, likely reflecting mildly increased tumbling times resulting from the motional drag that the bound IDP exerts (31).

The full EH-domain (EH123) binds NPF and non-NPF motifs efficiently.

Since the different EH domains are normally not isolated, but expressed in row in the context of Eps15, we investigated the interaction between $Dab2_{320-495}$ and the full EH-domain (EH1-EH2-EH3, also called EH123) and titrated increasing concentrations of EH123 into ^{15}N labeled $Dab2_{320-495}$. As expected from the interactions of the individual EH domains, both CSPs and $R_{1\rho}$ rates revealed that EH123 was able to interact with the the same five regions of $Dab2_{320-495}$ as observed for EH2 and EH3 (Figure 3A and B). Interestingly, the $R_{1\rho}$ relaxation rates of ^{15}N-$Dab2_{320-495}$ in the presence of EH123 show increased relaxation not only of the residues of the five $Dab2_{320-495}$ binding regions, but the residues located in between the binding motifs also show mildly increased rates. This is particularly evident for the residues located between the first three binding motifs (DYFDQQF, WPF and NPF) and suggests an overall stiffening of the chain, potentially due to binding of the motifs to different EH domains within the same EH123 molecule.

While CSPs around the NPF motif remain the largest upon interaction with EH123, as it is also the case when $Dab2_{320-495}$ interacts with the individual EH domains, the difference between the interaction of EH123 with the NPF motif and the other motifs appears smaller than for interaction with the individual EH domains, and indeed, $R_{1\rho}$ rates increase around these more promiscuous sites much more significantly. Binding affinities approximated from the CSPs for EH123 binding are significantly higher than those of the individual EH domains (Figure S7). This suggests that, when one EH domain within EH123 is bound to $Dab2_{320-495}$, the other two EH domains of the same molecule remain available for (preferential) binding to other motifs, an effect reminiscent of avidity, effectively increasing the total level of binding promiscuity. A much higher concentration of individual EH domains (3x as many) are needed to partially recover the chemical shift differences and ^{15}N $R_{1\rho}$ rates of $Dab2_{320-495}$ in the presence of EH123 (Figure S13A and B).

EH2 and EH3 tumble together in the context of the full EH-domain.

We also aimed to describe the interaction between $Dab2_{320-495}$ and EH123 from the side of EH123 and therefore produced EH123 ^{15}N labeled and recorded a ^{1}H-^{15}N HSQC spectrum of these combined EH domains. If the different EH domains were unaffected by being connected to the other EH domains, we would expect this spectrum to overlay perfectly with those of the individual EH domains. Surprisingly, the spectrum overlaid relatively well with the spectrum of EH1, but seemingly not with the spectra of EH2 and EH3, whose peaks were severely broadened. Nonetheless, weak peaks originating from EH2 and EH3 could also be identified in the spectrum of EH123, allowing the assignments from the individual domains to be fully transferred to the combined construct (Figure S14). In order to examine the broadening of the peaks originating from EH2 and EH3, we recorded ^{15}N spin relaxation of EH123 ($R_{1\rho}$ and hetNOEs). All $R_{1\rho}$ rates of EH123 were significantly increased as compared to the individual EH domains. The rates of EH2 and EH3, however, were significantly higher overall than those from EH1 within the EH123 construct (Figure 3C, S14C). Indeed, the increased $R_{1\rho}$ rates were the same for EH2 and EH3, which suggests that EH2 and EH3 tumble together as one entity, while EH1 can move independently within the full EH-domain. Heteronuclear NOEs, which are sensitive to much faster motion than $R_{1\rho}$ rates, in the picosecond range, show quite similar values all along EH123, reflecting the similar size and fold of the individual domains. Only the linker between EH1 and EH2 displays much lower hetNOE values, demonstrating that this linker was undergoing much more rapid motion than the rest of the protein construct. The linker connecting EH2 and EH3 does not seem

to move as much on those fast time scales, in very good agreement with EH2 and EH3 tumbling together within the EH123 construct.

When $Dab2_{320-495}$ was added to ^{15}N labeled EH123, we observed chemical shift displacements similar to those of the individual EH domains when interacting with $Dab2_{320-495}$ (Figure 3D), suggesting that the binding sites on all EH domains are available also within EH123, despite the fact that EH2 and EH3 tumble together and potentially interact within this construct. ^{15}N $R_{1\rho}$ rates increased throughout EH123 when $Dab2_{320-495}$ was added, while the rates of EH1 still remain lower than those of EH2 and EH3, showing that binding of $Dab2_{320-495}$ does not impair the arrangement of the EH domains within EH123.

Eps15's own IDR interacts with EH123 and partially competes with $Dab2_{320-495}$ binding.

Eps15 has recently been shown to undergo liquid-liquid phase separation and this mechanism was proposed to be key to the initiation of clathrin-mediated endocytosis (22). Even though NPF motifs, known to be the main binding sites for EH domains contained in Eps15 (32), are not present in Eps15's own IDR ($Eps15_{IDR}$), we wanted to test whether EH123 could still bind to $Eps15_{IDR}$, motivated by the remarkable binding promiscuity observed between EH domains and $Dab2_{320-495}$. Eps15 tetramers have previously been observed and seem to require both EH domains as well as the intrinsically disordered domain (13). When we added equimolar concentrations of $Eps15_{IDR}$ to ^{15}N labeled EH123, we indeed saw chemical shift perturbations throughout the EH123 domain ^{1}H-^{15}N HSQC spectrum, similar to those observed upon addition of $Dab2_{320-495}$, and suggesting that all EH domains are affected by an interaction with $Eps15_{IDR}$. ^{15}N $R_{1\rho}$ rates of EH123 are increased throughout the EH domain upon $Eps15_{IDR}$ interaction (Figure 4D).

The interaction observed between EH123 and $Eps15_{IDR}$ suggests that intramolecular interactions within Eps15 may occupy NPF binding sites in the EH domain in the native context. To test this, we conducted a competition experiment, acquiring a spectrum of ^{15}N EH123 with equimolar amounts of both $Eps15_{IDR}$ and $Dab2_{320-495}$. CSPs of EH123 in the presence of both $Dab2_{320-495}$ and $Eps15_{IDR}$ were similar to those in the presence of $Dab2_{320-495}$ and $Eps15_{IDR}$ alone (Figure 4D), suggesting that either one of the IDRs ($Dab2_{320-495}$ or $Eps15_{IDR}$) or both were bound. To asses these possibilities, we recorded a ^{1}H-^{15}N HSQC spectrum of the ^{15}N labeled $Eps15_{IDR}$ and added first EH123 and then $Dab2_{320-495}$ (Figure 4BC). Several peaks of the ^{15}N labeled Eps15 shifted or disappeared in the presence of EH123, clearly showing the interaction between EH domains and $Eps15_{IDR}$. When $Dab2_{320-495}$ was added in addition, many peaks that were already broadened because of EH123 binding, broadened even further. This could be explained by the increased tumbling times of the complex when $Dab2_{320-495}$ was bound to EH123 in addition to $Eps15_{IDR}$, and suggests that a trimeric complex can be formed. Some peaks of the $Eps15_{IDR}$ ^{1}H-^{15}N HSQC spectrum, however, shifted in the presence of EH123 and then reverted to their original position, when $Dab2_{320-495}$ was added, suggesting partially competitive interactions (Figure 4B and C). Which regions are competed off and which ones remain bound in the presence of $Dab2_{320-495}$ will eventually be determined by the relative affinities of the different motifs that are prone to bind to the EH domains.

Discussion

The dynamic network formed by intrinsically disordered regions (IDRs) and folded proteins interacting with short linear motifs within IDRs, is key to a number of biological processes (4, 33). Clathrin mediated endocytosis is a prime example for a process that comprises many of those short linear motifs (2, 20), leading to the formation of a complex interaction network. Known examples are the α and β2 appendage domains of the major adaptor ptotein AP2 that interact with DPF/DPW and FxDxF motifs (x = any amino acid) (3), the clathrin heavy chain terminal domain, known to interact with DLL and DLF motifs (7, 8) or the EH domains found in Eps15, which interact with NPF motifs of diverse IDR partners (17). Although extensive studies have identified these consensus sequences, it has meanwhile become clear that additional binding sites are yet to be discovered and this requires a strategy by which focus lies on studying long endocytic IDRs. This has recently allowed identifying a particularly long interaction site between the neuronal AP180 and the AP2 β2 appendage domain (7). In addition, many endocytic IDRs seem to bind to the same partners (34) and understanding how the different binding modes synergize or compete with each other is crucial for a molecular comprehension of clathrin mediated endocytosis.

In this study, we shed light onto those partially competitive interactions by investigating binding of a large intrinsically disordered region stemming from the CLASP Dab2 ($Dab2_{320-495}$) and its interactions with Eps15 EH domains, as well as its competition for binding with Eps15's own IDR ($Eps15_{IDR}$). In line with the previous literature and extensive peptide screens to assess binding patterns of Eps15 EH domains (32), all three EH domains of Eps15 (EH1, EH2 and EH3) prefer to bind to the only NPF motif within the sequence of $Dab2_{320-495}$ (Figure 1 and 2). In particular in the presence of EH2, significant exchange in the microsecond to millisecond time scale is observed around the NPF motif and an N-terminal transient helix in $Dab2_{320-495}$ ($helix_N$), allowing to estimate a dissociation constant between $Dab2_{320-495}$ on the order or hundreds of micromolar (Figure 2 and Figure S7). These affinities are in agreement with affinities of other small linear motif interactions determined in the context of clathrin mediated endocytosis (7–9), but orders of magnitudes weaker than those observed between Stonin2 and EH2 (K_D in the nanomolar range) (17). We further observed extremely promiscuous binding behavior for EH2 and EH3, also involving DYF, WPF, DLF, and DIF motifs, albeit with a lower apparent affinity (Figure 1). This is in line with the observation that other EH domains, such as the EH domain of EHD1 or of POB-1 can bind to the motif xPF (35, 36). By investigating the EH domain interactions with small linear motifs from the side of a bona fide IDR, we can conclude that the promiscuity of interaction motifs is even larger than previously anticipated, binding to most phenylalanine containing motifs.

Even though some proteins contain individual EH domains, this is not the case for Eps15, which contains EH1, EH2 and EH3 sequentially at its N-terminus. Unexpectedly, we observe that EH2 and EH3 move together as one entity in a construct comprising all three EH domains (EH123, Figure 3C), suggesting a potential interaction between EH2 and EH3. EH1, on the other hand, tumbles independently from the other two EH domains. Nonetheless, EH123 makes its binding sites available for interaction with $Dab2_{320-495}$. From the side of $Dab2_{320-495}$, binding to EH123 is strikingly different than binding to the individual EH domains. While the same NPF and promiscuous motif interactions maintain, the non-NPF interactions seem to gain importance, possibly enhanced through avidity effects of the three EH domains in close spatial proximity compared to the individual domains (Figure 3, S13).

The present promiscuity of interactions, particularly in the context of interaction with the full EH123 construct, suggests that the EH domains might be binding to Eps15's own IDR, which has also been suggested previously (13, 22, 36). Addition of $Eps15_{IDR}$ to ^{15}N labeled EH123 led indeed to chemical shift perturbations and slightly increased ^{15}N transverse relaxation rates confirming this intramolecular interaction. When both $Eps15_{IDR}$ and $Dab2_{320-495}$ are added to EH123, the binding signature is not very different from the one when only one of the IDRs (Dab2 or Eps15) is bound. Viewed from the side of $Dab2_{320-495}$ or from the side of $Eps15_{IDR}$, however, an interesting observation can be made: While ^{15}N $R_{1\rho}$ rates of $Dab2_{320-495}$ increase around the NPF motif and the other promiscuous motifs when EH123 is present, suggesting binding and therefore slowed tumbling times around these interaction sites, the rates increase even further when $Eps15_{IDR}$ is added in addition, arguing for an even slower tumbling and thus the formation of a trimeric complex (Figure 4E). How is this possible when $Dab2_{320-495}$ and $Eps15_{IDR}$ occupy the same binding sites on EH123? Key to this question is likely the multivalency by which both IDRs interact with EH123, such that, while some motifs of $Dab2_{320-495}$ might be displaced from EH123 in a dynamic fashion when $Eps15_{IDR}$ is added, others maintain. The same seems to be true when $Eps15_{IDR}$ is ^{15}N labeled and EH123 and then $Dab2_{320-495}$ are added, where most chemical shift perturbations that occurred during binding of EH123 maintain, while others revert to the unbound state (Figure 4B and C), probably displaced by competition with $Dab2_{320-495}$. Which of the motifs remain bound to EH123 and which get displaced is certainly a function of the individual motif's affinities. This is easiest visualized as a dynamic equilibrium where motifs in Dab2 are competing with Eps15's own IDR for binding to the EH domains, forming a complex and dynamic network (Figure 5). The fact that a trimeric complex between $Dab2_{320-495}$, $Eps15_{IDR}$ and EH123 can be formed while using the same binding sites of EH123, suggests that the strengths of the interactions between EH123 and $Dab2_{320-495}$ or EH123 and $Eps15_{IDR}$ are not vastly different, even though Eps15 IDR presents many more promiscuous interaction motifs than $Dab2_{320-495}$. This argues for a physiological relevance of the interactions seen between the EH domains and $Eps15_{IDR}$ and the competition effects observed.

While binding of EH domains to an intrinsically disordered linker of the same protein has been observed for the EH domain contained in EHD2 (37), the interaction network established by Eps15 is certainly remarkable, since so many interactions take place and compete with each other (Figure 5). This has implications for all other binding partners of Eps15, whether binding to the EH domains or Eps15's IDR, since any binding partner will be competing with these intra-molecular interactions. Indeed, the interactions observed between Eps15 EH domains and $Eps15_{IDR}$ could constitute some kind of auto-inhibitory mechanism, such as recently described for WW domain proteins (38), that could be (partially) released by NPF containing proteins, such as Dab2 Based on previous literature on the interaction between the EH domain of POB1 and DPF motifs , which are also contained in $Eps15_{IDR}$, interaction between Eps15 EH domains and $Eps15_{IDR}$ have been suggested to be important for liquid-liquid phase separation in the context of clathrin mediated endocytosis (22). In this context it should be noted, that the interactions observed here between EH123 and $Eps15_{IDR}$ could be both intra-molecular within one Eps15 molecule or inter-molecular between different Eps15 molecules. Indeed, it will be interesting to see, whether the interactions between EH domains and $Eps15_{IDR}$ are maintained also in the presence of other and more NPF containing proteins, binding with higher affinities (17), and what consequences this has on liquid-liquid phase separation at the endocytic pit and thus progression of productive endocytosis.

Materials and Methods

Cloning

Eps15-pmCherryN1 was a gift from Christien Merrifield (Addgene plasmid # 27696 ; http://n2t.net/addgene:27696 ; RRID:Addgene_27696) (39). The three individual EH domains (EH1, EH2, EH3) were cloned into the pET41c vector leading to constructs with a non-cleavable C-terminal His-tag. The full EH domain (EH123) and $Eps15_{IDR}$ were cloned into the pET28a vector with an N-terminal GB1 solubility tag pET28-6His-GB1. This leads to the expression of a TEV (tobacco etch virus) cleavable 6His-GB1-TEV site construct followed by the protein of interest. The gene of $Dab2_{320-495}$ was purchased from Twist Bioscience and cloned into a pET28a vector with non-cleavable C-terminal His-tag. $Dab2_{328-360}$ and $Dab2_{358-390}$ were cloned into a pET28a vector with an N-terminal GB1 solubility tag pET28-6His-GB1.

Protein expression and purification

The proteins were expressed in the *E. coli* Rosetta (DE3) and grown in LB medium with Kanamycin and Chloramphenicol at 37°C. When the optical density (OD) at 600 nm was around 0.6-1, expression was induced with 1 mM isopropyl-β-D-thiogalactopyranoside (IPTG) and the expression was then continued at 20°C over night. For isotope labeling (^{15}N, ^{13}C) M9 minimal medium was used and supplemented with 1g/L $^{15}NH_4Cl$ and/or with 2 g/l ^{13}C-glucose.

Cells were lysed by sonication in lysis buffer (20 mM Tris, 150 mM NaCl pH 8, with Roche Ethylenediaminetetraacetic Acid (EDTA)-free protease inhibitor cocktail (Sigma-Aldrich Chemie GmbH)). Purification involved a two-step process: initial nickel purification followed by Size-Exclusion Chromatography (SEC). The nickel column was equilibrated in lysis buffer before the filtered lysate was applied to a nickel column. The column was then washed in lysis buffer containing 20 mM imidazole, and the protein was eluted using lysis buffer supplemented with 400 mM imidazole. For all constructs expressed in the pET28-6His-GB1 vector, the eluted fraction, which contained the target protein (validated via SDS-PAGE and Coomassie staining), underwent overnight dialysis at 4°C in 500 mL of lysis buffer supplemented with 5 mM β-mercaptoethanol and 1 mg TEV protease before proceeding to the SEC purification step. Proteins were further purified using a Superdex 75 column, equilibrated in NMR buffer (50 mM Na-phosphate pH 6, 150 mM NaCl, and 2 mM dithiothreitol (DTT)). Fractions containing pure protein (by SDS-PAGE) were concentrated and frozen with final protein concentrations determined by absorbance at 280nm using extinction coefficients determined by Expasy Protparam (40).

NMR spectroscopy

NMR experiments were measured at the Leibniz-Forschungsinstitut für Molekulare Pharmakologie (FMP), Berlin, Germany (^{1}H frequencies of 600, 750, 900 MHz). All experiments were measured in NMR buffer (50 mM Na-phosphate pH 6, 150 mM NaCl, 2 mM DTT) at 25°C. Addition of up to 5 mM $CaCl_2$ did not affect our results. Spectra were processed with NMRPipe (41), using qMDD for non-uniformly sampled spectra, and analyzed with CCPN (42).

$^{15}N/^{13}C$ Backbone assignment

Almost complete assignments could be obtained for all the constructs. The assignment spectra of the $^{15}N/^{13}C$ labelled constructs were acquired at a ^{1}H frequency of 750 MHz, except for those of $Dab2_{320-495}$ wich were

acquired at 600 MHz. Standard BEST-TROSY triple resonance experiments correlating CO, Cα, Cβ resonances (HNCO, HNCOCA, HNCA, iHNCA, HNCOCACB, iHNCACB) (43) were acquired. The assignments were done in CCPN and then validated using MARS (44). Secondary chemical shifts and secondary structure propensities (SSPs (45)) were calculated using random coil values from refDB (46). Overlapping the 3 TROSY spectra of the individual EH domains (EH1, EH2, EH3) we transferred the ^{1}H and ^{15}N resonances to the TROSY of the combined EH123 domain.

^{15}N relaxation, relaxation dispersion and titrations

Extraction of peak intensities (I) as well as ^{1}H and ^{15}N chemical shifts, were carried out from ^{1}H-^{15}N HSQC or BEST-TROSY spectra. Combined chemical shift perturbations (CSPs) were calculated using

$$CSP=\sqrt{(\delta^{1}H\cdot 6.5)^{2}+(\delta^{15}N)^{2}} \quad (1)$$

Concentrations used are indicated in the respective figures.

Residue specific K_d values were estimated by fitting the following equation to the CSPs as a function of concentration:

$$\Delta CSP=\Delta CSP_{max}\cdot\frac{[Dab2]+[EHx]+Kd-\sqrt{([Dab2]+[EHx]+Kd)^{2}-4\cdot[Dab2]\cdot[EHx]}}{2\cdot[Dab2]}$$

Fitting was performed with Python.

^{15}N $R_{1\rho}$, R_1 and {^{1}H}-^{15}N HetNOE relaxation rates (47) were assessed at 600 MHz ^{1}H Larmor frequency. The spin-lock field for the $R_{1\rho}$ experiment was set to 1500 Hz, and 6-7 delays, between 10 and 230 ms (for the disordered Dab2$_{320-495}$) and between 10 and 70 ms (for the folded EH domains) were used to sample the decay of magnetization. R_1 was measured using 6-7 delays between 0 to 1.2 s.

Relaxation dispersion experiments (48) were conducted at 600 and 900 MHz, employing 14 CPMG frequencies ranging from 31 to 1000 Hz, with a constant-time relaxation of 32 ms. Errors were determined based on standard deviations of repeat measurements. The minimum error was set to 0.5. For the experiment with 100 µM Dab2$_{320-495}$ in the presence of 10% EH2, 12 residues within the helix$_N$ and the NPF motif were fit globally using a 2 site exchange model with the software ChemEx (https://github.com/gbouvignies/chemex). An exchange rate of 149 ± 13 s^{-1} and a percentage bound of 3 ± 0.3% were obtained from the fit.

Conformational ensemble of Dab2$_{320-495}$

A conformational ensemble was calculated from Dab2$_{320-495}$ and Dab2$_{328-360}$ using a combination of the statistical coil generator flexible meccano (23) and the genetic algorithm ASTEROIDS (24). From a statistical coil ensemble of 10,000 conformers, 200 conformations that together best described the H$_N$, N, CO, Cα and Cβ chemical shifts of the proteins were selected. A new ensemble of 8500 conformers was generated using the Φ and ψ angles from the previous selection and supplemented with 1500 conformations from the previous pool of conformers. A new selection of 200 conformations was performed on the new pool. This iteration was repeated 4 times. Ensemble averaged chemical shifts were generated using SPARTA (48) and secondary chemical shifts were calculated based on RefDB (46).

Structures of the individual EH domains

The structures that were used to plot the chemical shift perturbations (CSPs) for EH2 and EH3 are the PDB codes 1FF1 (29) and 1C07 (30) respectively. For the first EH domain we use an AlphaFold (50, 51) prediction since no *human* Eps15 EH1 structure is deposited in the PDB. The CSPs of 100 µM Dab2$_{320-495}$

were plotted onto the structures. The linear gradient is from 0%, which represents no CSP, up to 100%, which is the highest CSP observed at 0.75 ppm. The structures were visualized using Pymol (52).

Data, Materials, and Software Availability

The assignment of $Dab2_{320-495}$ has been uploaded to the Biological Magnetic Resonance Data Bank (BMRB) under the accession number 52613.

Acknowledgments

We thank all members of the Milles group for fruitful discussions and critical proofreading. We thank M.R. Jensen for providing the pET28-6His-GB1 plasmid, M. Blackledge and M.R. Jensen for providing analysis scripts, and P. Schmieder, N. Trieloff and M. Beerbaum for technical assistance on the NMR spectrometers. The Institut de Biologie Structurale acknowledges integration into the Interdisciplinary Research Institute of Grenoble. This work was supported by the Leibniz-Forschungsinstitut für Molekulare Pharmakologie (FMP) (to S.M.). This project has received funding from the European Research Council (ERC) Starting Grant MultiMotif to S.M. under the European Union's Horizon 2020 research and innovation program (grant agreement no. 802209).

References

1. M. Kaksonen, A. Roux, Mechanisms of clathrin-mediated endocytosis. *Nat Rev Mol Cell Biol* **19**, 313–326 (2018).
2. L. Maldonado-Báez, B. Wendland, Endocytic adaptors: recruiters, coordinators and regulators. *Trends Cell Biol* **16**, 505–513 (2006).
3. T. J. Brett, L. M. Traub, D. H. Fremont, Accessory protein recruitment motifs in clathrin-mediated endocytosis. *Structure* **10**, 797–809 (2002).
4. K. Van Roey, *et al.*, Short Linear Motifs: Ubiquitous and Functionally Diverse Protein Interaction Modules Directing Cell Regulation. *Chem. Rev.* **114**, 6733–6778 (2014).
5. E. M. Schmid, *et al.*, Role of the AP2 beta-appendage hub in recruiting partners for clathrin-coated vesicle assembly. *PLoS Biol* **4**, e262 (2006).
6. G. J. K. Praefcke, *et al.*, Evolving nature of the AP2 alpha-appendage hub during clathrin-coated vesicle endocytosis. *EMBO J* **23**, 4371–4383 (2004).
7. S. Naudi-Fabra, *et al.*, An extended interaction site determines binding between AP180 and AP2 in clathrin mediated endocytosis. *Nat Commun* **15**, 5884 (2024).
8. Y. Zhuo, *et al.*, Dynamic Interactions between Clathrin and Locally Structured Elements in a Disordered Protein Mediate Clathrin Lattice Assembly. *J Mol Biol* **404**, 274–290 (2010).
9. Y. Zhuo, *et al.*, Nuclear Magnetic Resonance Structural Mapping Reveals Promiscuous Interactions between Clathrin-Box Motif Sequences and the N-Terminal Domain of the Clathrin Heavy Chain. *Biochemistry* **54**, 2571–2580 (2015).

10. W. M. Henne, *et al.*, FCHo proteins are nucleators of clathrin-mediated endocytosis. *Science* **328**, 1281–1284 (2010).
11. S. Confalonieri, P. P. Di Fiore, The Eps15 homology (EH) domain. *FEBS Letters* **513**, 24–29 (2002).
12. F. Tebar, S. Confalonieri, R. E. Carter, P. P. Di Fiore, A. Sorkin, Eps15 Is Constitutively Oligomerized Due to Homophilic Interaction of Its Coiled-coil Region*. *Journal of Biological Chemistry* **272**, 15413–15418 (1997).
13. P. Cupers, E. ter Haar, W. Boll, T. Kirchhausen, Parallel dimers and anti-parallel tetramers formed by epidermal growth factor receptor pathway substrate clone 15. *J Biol Chem* **272**, 33430–33434 (1997).
14. P. M. van Bergen en Henegouwen, Eps15: a multifunctional adaptor protein regulating intracellular trafficking. *Cell Communication and Signaling* **7**, 24 (2009).
15. A. Reider, *et al.*, Syp1 is a conserved endocytic adaptor that contains domains involved in cargo selection and membrane tubulation. *EMBO J* **28**, 3103–3116 (2009).
16. A. E. Salcini, *et al.*, Binding specificity and in vivo targets of the EH domain, a novel protein–protein interaction module. *Genes Dev* **11**, 2239–2249 (1997).
17. J. Rumpf, *et al.*, Structure of the Eps15-stonin2 complex provides a molecular explanation for EH-domain ligand specificity. *EMBO J* **27**, 558–569 (2008).
18. A. Teckchandani, E. E. Mulkearns, T. W. Randolph, N. Toida, J. A. Cooper, The clathrin adaptor Dab2 recruits EH domain scaffold proteins to regulate integrin β1 endocytosis. *Mol Biol Cell* **23**, 2905–2916 (2012).
19. C. V. Finkielstein, D. G. S. Capelluto, Disabled-2: A modular scaffold protein with multifaceted functions in signaling. *Inside the Cell* **1**, 48–58 (2016).
20. S. M. Smith, M. Baker, M. Halebian, C. J. Smith, Weak Molecular Interactions in Clathrin-Mediated Endocytosis. *Frontiers in Molecular Biosciences* **4** (2017).
21. K. Takei, V. Haucke, Clathrin-mediated endocytosis: membrane factors pull the trigger. *Trends in Cell Biology* **11**, 385–391 (2001).
22. K. J. Day, *et al.*, Liquid-like protein interactions catalyse assembly of endocytic vesicles. *Nat Cell Biol* **23**, 366–376 (2021).
23. V. Ozenne, *et al.*, Flexible-meccano: a tool for the generation of explicit ensemble descriptions of intrinsically disordered proteins and their associated experimental observables. *Bioinformatics* **28**, 1463–1470 (2012).
24. M. R. Jensen, L. Salmon, G. Nodet, M. Blackledge, Defining conformational ensembles of intrinsically disordered and partially folded proteins directly from chemical shifts. *J Am Chem Soc* **132**, 1270–1272 (2010).
25. J. Rumpf, B. Simon, Y. Groemping, M. Sattler, 1H, 13C, and 15N chemical shift assignments for the Eps15-EH2-stonin 2 complex. *Biomol NMR Assign* **2**, 55–58 (2008).
26. A. Carotenuto, *et al.*, Sequence-specific 1H, 13C and 15N assignment and secondary structure of the apo EH2 domain of mouse Eps15. *J Biomol NMR* **14**, 97–98 (1999).
27. B. Whitehead, *et al.*, Sequence-specific 1H, 13C and 15N assignment of the EH1 domain of mouse Eps15. *J Biomol NMR* **12**, 465–466 (1998).

28. B. Whitehead, M. Tessari, A. Carotenuto, P. M. P. van Bergen en Henegouwen, G. W. Vuister, The EH1 Domain of Eps15 Is Structurally Classified as a Member of the S100 Subclass of EF-Hand-Containing Proteins. *Biochemistry* **38**, 11271–11277 (1999).
29. T. de Beer, *et al.*, Molecular mechanism of NPF recognition by EH domains. *Nat Struct Biol* **7**, 1018–1022 (2000).
30. J. L. Enmon, T. de Beer, M. Overduin, Solution Structure of Eps15's Third EH Domain Reveals Coincident Phe−Trp and Asn−Pro−Phe Binding Sites,. *Biochemistry* **39**, 4309–4319 (2000).
31. S.-H. Bae, H. J. Dyson, P. E. Wright, Prediction of the rotational tumbling time for proteins with disordered segments. *J Am Chem Soc* **131**, 6814–6821 (2009).
32. S. Paoluzi, *et al.*, Recognition specificity of individual EH domains of mammals and yeast. *The EMBO Journal* **17**, 6541–6550 (1998).
33. H. Y. J. Fung, M. Birol, E. Rhoades, IDPs in macromolecular complexes: the roles of multivalent interactions in diverse assemblies. *Curr Opin Struct Biol* **49**, 36–43 (2018).
34. D. Duan, M. Hanson, D. O. Holland, M. E. Johnson, Integrating protein copy numbers with interaction networks to quantify stoichiometry in clathrin-mediated endocytosis. *Sci Rep* **12**, 5413 (2022).
35. F. Kieken, *et al.*, Structural insight into the interaction of proteins containing NPF, DPF, and GPF motifs with the C-terminal EH-domain of EHD1. *Protein Science* **18**, 2471–2479 (2009).
36. E. Santonico, S. Panni, M. Falconi, L. Castagnoli, G. Cesareni, Binding to DPF-motif by the POB1 EH domain is responsible for POB1-Eps15 interaction. *BMC Biochemistry* **8**, 29 (2007).
37. O. Daumke, *et al.*, Architectural and mechanistic insights into an EHD ATPase involved in membrane remodelling. *Nature* **449**, 923–927 (2007).
38. S. Martínez-Lumbreras, *et al.*, Intramolecular autoinhibition regulates the selectivity of PRPF40A tandem WW domains for proline-rich motifs. *Nat Commun* **15**, 3888 (2024).
39. M. J. Taylor, D. Perrais, C. J. Merrifield, A High Precision Survey of the Molecular Dynamics of Mammalian Clathrin-Mediated Endocytosis. *PLOS Biology* **9**, e1000604 (2011).
40. E. Gasteiger, *et al.*, "Protein Identification and Analysis Tools on the ExPASy Server" in *The Proteomics Protocols Handbook*, J. M. Walker, Ed. (Humana Press, 2005), pp. 571–607.
41. F. Delaglio, *et al.*, NMRPipe: a multidimensional spectral processing system based on UNIX pipes. *J Biomol NMR* **6**, 277–293 (1995).
42. S. P. Skinner, *et al.*, CcpNmr AnalysisAssign: a flexible platform for integrated NMR analysis. *J Biomol NMR* **66**, 111–124 (2016).
43. Z. Solyom, *et al.*, BEST-TROSY experiments for time-efficient sequential resonance assignment of large disordered proteins. *J Biomol NMR* **55**, 311–321 (2013).
44. Y.-S. Jung, M. Zweckstetter, Mars -- robust automatic backbone assignment of proteins. *J Biomol NMR* **30**, 11–23 (2004).
45. J. A. Marsh, V. K. Singh, Z. Jia, J. D. Forman-Kay, Sensitivity of secondary structure propensities to sequence differences between α- and γ-synuclein: Implications for fibrillation. *Protein Sci* **15**, 2795–2804 (2006).
46. H. Zhang, S. Neal, D. S. Wishart, RefDB: a database of uniformly referenced protein chemical shifts. *J Biomol NMR* **25**, 173–195 (2003).

47. N.-A. Lakomek, J. Ying, A. Bax, Measurement of 15N relaxation rates in perdeuterated proteins by TROSY-based methods. *J Biomol NMR* **53**, 209–221 (2012).
48. D. F. Hansen, P. Vallurupalli, L. E. Kay, An improved 15N relaxation dispersion experiment for the measurement of millisecond time-scale dynamics in proteins. *J Phys Chem B* **112**, 5898–5904 (2008).
49. Y. Shen, A. Bax, Protein backbone chemical shifts predicted from searching a database for torsion angle and sequence homology. *J Biomol NMR* **38**, 289–302 (2007).
50. J. Jumper, *et al.*, Highly accurate protein structure prediction with AlphaFold. *Nature* **596**, 583–589 (2021).
51. M. Mirdita, *et al.*, ColabFold: making protein folding accessible to all. *Nat Methods* **19**, 679–682 (2022).
52. The PyMOL Molecular Graphics System, Version 3.0 Schrödinger, LLC.
53. G. Erdős, Z. Dosztányi, Analyzing Protein Disorder with IUPred2A. *Current Protocols in Bioinformatics* **70**, e99 (2020).

Figures

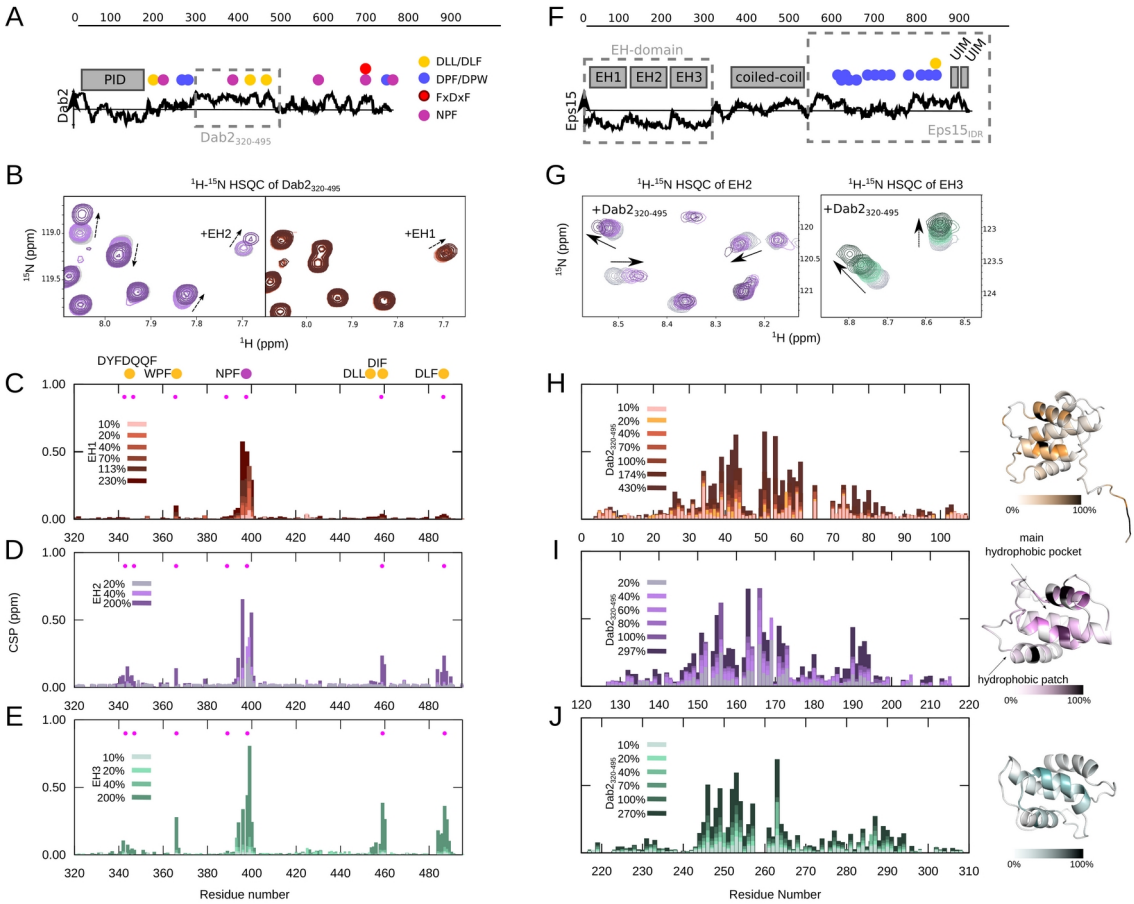

Figure 1. Interaction between Dab2$_{320-495}$ and the individual EH domains from Eps15. (A) Scheme of Dab2. The disorder prediction (IUPred (53)) is shown as a black curve along the sequence. Positive: predicted disordered, negative: predicted ordered. 0 is the straight black line. The folded domain (PID: phoshotyrosine interacting domain) is shown as a gray box above the disorder prediction. Putative interaction motifs are shown as colored circles along the sequence (legend on the right). DLL/DLF: clathrin binding; DPF/DPW: AP2α binding; FxDxF: AP2β binding; NPF: EH domain binding. The construct used in the study is boxed with a gray dashed line. **(B)** Zoom into a ^{1}N-^{15}N HSQC spectrum of Dab2$_{320-495}$ in the absence and presence of EH2 (left) and EH1 (right). **(C) – (E)** Chemical shift perturbations (CSPs) of 100 µM Dab2$_{320-495}$ in the presence versus the absence of increasing concentrations of EH1 (C), EH2 (D) and EH3 (E), respectively. Color legends are displayed in the respective plots. Unfilled pink circles denote positions of phenylalanines. **(F)** Scheme of Eps15. The disorder prediction is shown as a black curve along the sequence as in (A). Gray boxes refer to folded elements: EH (Eps15-homology) domains 1-3, the coiled-coil domain, and ubiquitin interaction motifs (UIMs). Putative binding motifs are shown in colored circles (legend in (A)). The constructs used in the study is boxed with a gray dashed line. Constructs of EH1, EH2 and EH3 are also used individually. **(G)** Zoom into a ^{1}N-^{15}N HSQC spectrum of EH2 (left) and EH3 (right) in the presence of Dab2$_{320-495}$. **(H) – (J)** CSPs of 100 µM EH1 (H), EH2 (I) and EH3 (J), respectively, in the absence versus the presence of increasing amounts of Dab2$_{320-495}$. Color legends are displayed in the respective plots. Structures

of EH1 (Alphafold (50, 51)), EH2 (PDB 1FF1 (29)) and EH3 (PDB 1C07 (30)) are displayed to the right of the CSP plots with the CSP at 100% $Dab2_{320-495}$ mapped on to them. The linear gradient starts from 0% (white) which represents no CSP, and the 100% (black) is 0.75 ppm which is the highest CSP observed between EH2 and $Dab2_{320-495}$. All experiments were acquired at 25°C.

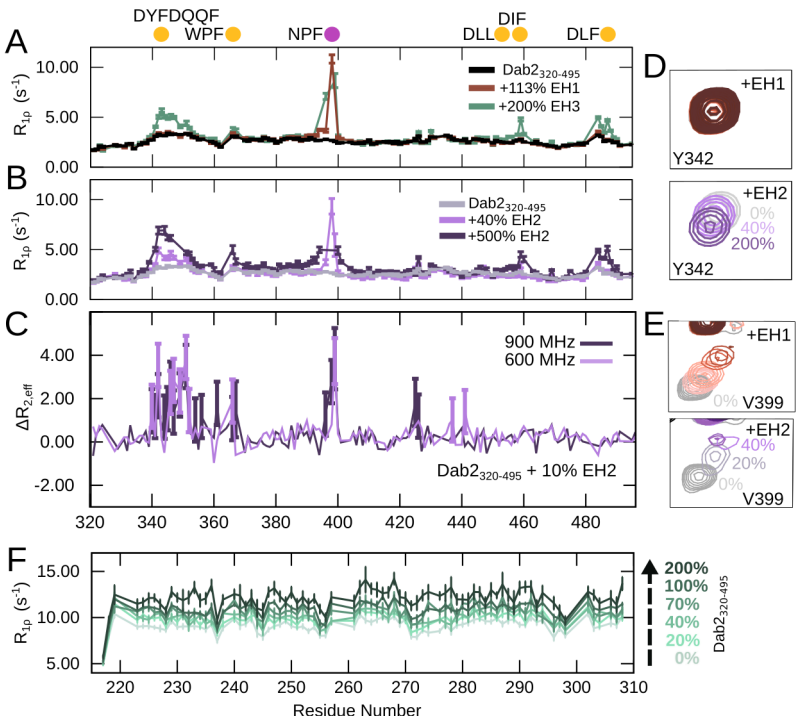

Figure 2. ^{15}N spin relaxation of Dab2$_{320-495}$ and EH domains upon interaction. (A) ^{15}N $R_{1\rho}$ spin relaxation of Dab2$_{320-495}$ (100 µM) in the absence and presence of EH1 and EH3 at a ^{1}H frequency of 600 MHz. **(B)** ^{15}N $R_{1\rho}$ spin relaxation of Dab2$_{320-495}$ (100 µM) in the absence and presence of increasing concentrations of EH2 and at a ^{1}H frequency of 600 MHz. **(C)** $\Delta R_{2,eff}$ calculated from effective R_2 values ($R_{2,eff}$) of relaxation dispersion experiments at a CPMG frequency of 31 Hz subtracted with $R_{2,eff}$ at a CPMG frequency of 1000 Hz of 100 µM Dab2$_{320-495}$ in the presence of 10% EH2. Experiments were recorded at a ^{1}H frequency of 600 MHz (light purple) and 900 MHz (dark purple). Error bars, propagated from the errors of $R_{2,eff}$ at 31 Hz and 1000 Hz, are shown for values that are significantly larger than 0 (compared to the error). **(D)** Zoom into the peak corresponding to Y342 from Dab2$_{320-495}$ ^{1}H-^{15}N HSQC spectra alone and in the presence of increasing concentrations of EH1 (top) and EH2 (bottom). **(E)** Zoom into the peak corresponding to V399 from Dab2$_{320-495}$ ^{1}H-^{15}N HSQC spectra alone and in the presence of increasing concentrations of EH1 (top) and EH2 (bottom). Color legend as in Figure 1C and D. **(F)** ^{15}N $R_{1\rho}$ spin relaxation of EH3 (100 µM) in the absence and presence of Dab2$_{320-495}$ at a ^{1}H frequency of 600 MHz. Color legends are indicated in the figures.

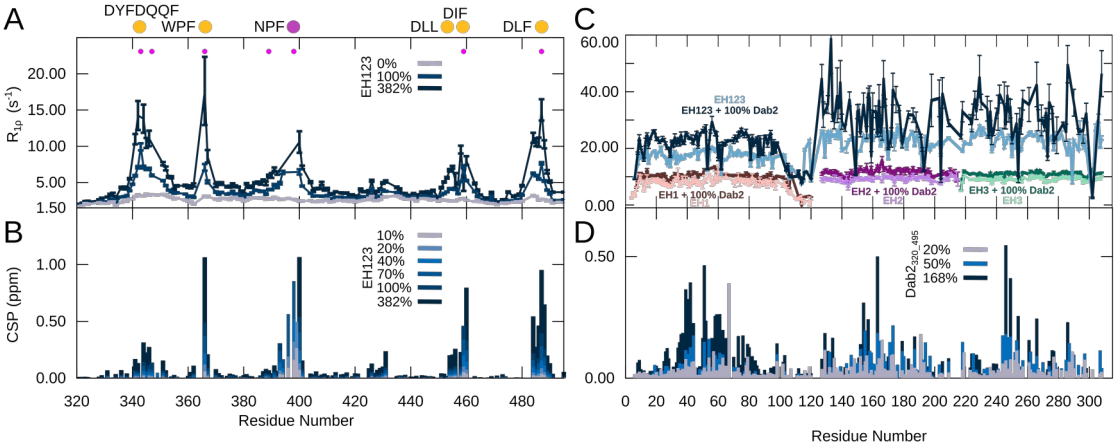

Figure 3. Interaction between EH1-EH2-EH3 (EH123) and Dab2$_{320-495}$. (A) ^{15}N $R_{1\rho}$ spin relaxation of Dab2$_{320-495}$ (100 µM) in the absence and presence of increasing concentrations of EH123 at a ^{1}H frequency of 600 MHz. **(B)** Combined CSPs between the ^{1}H-^{15}N HSQC of ^{15}N Dab2$_{320-495}$ in the presence of increasing amounts of EH123. The pink dots represent the Phe present in the Dab2$_{320-495}$. **(C)** ^{15}N $R_{1\rho}$ spin relaxation of the individual ^{15}N EH domains (EH1, EH2, EH3) as well as the full ^{15}N EH123 (200 µM) in the absence and presence of Dab2$_{320-495}$ at a ^{1}H frequency of 600 MHz. **(D)** Combined CSPs between the ^{1}H-^{15}N HSQC of the full ^{15}N EH123 domain in the presence of increasing amounts of the Dab2$_{320-495}$. The colors are indicated in the figures.

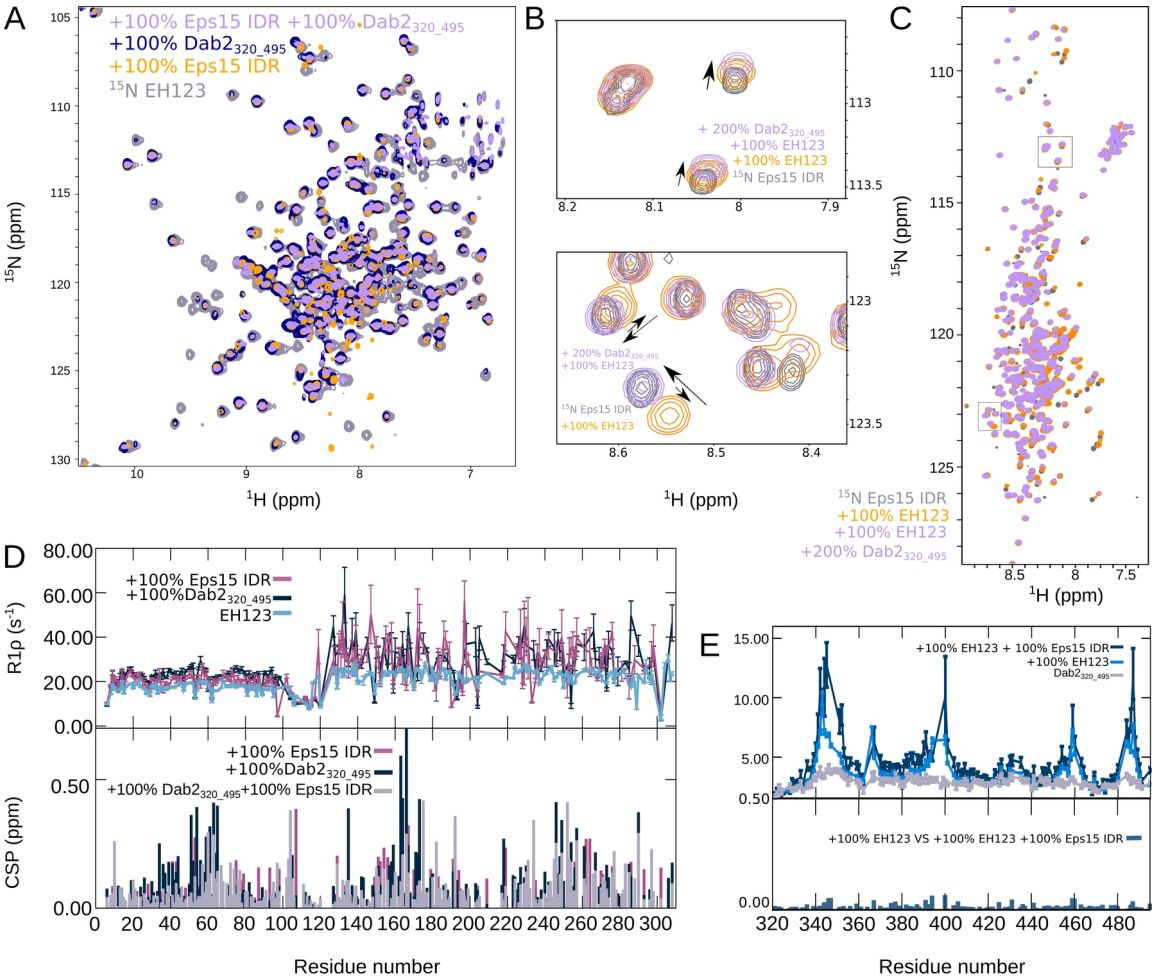

Figure 4: Competitive binding of Dab2 and Eps15 to the EH-domain (EH123). (A) ^{1}H-^{15}N TROSY spectrum of the EH-domain (EH123) alone (200 µM) and in the presence of Dab2$_{320\text{-}495}$, Eps15's IDR and a mix of Dab2$_{320\text{-}495}$ and Eps15's IDR. The colors are indicated in the figure. **(B)** Zoom into the spectra from (C), showing partial competition between Eps15's IDR and Dab2$_{320\text{-}495}$ binding to EH123. **(C)** ^{1}H-^{15}N HSQC spectrum of Eps15$_{IDR}$ alone (gray, 100 µM) and in the presence of EH123 (orange, 100 µM Eps15$_{IDR}$, 100 µM EH123) and EH123 and Dab2$_{320\text{-}495}$ (violet, 100 µM Eps15$_{IDR}$, 100 µM EH123, 200 µM Dab2$_{320\text{-}495}$). **(D)** ^{15}N $R_{1\rho}$ spin relaxation of the individual ^{15}N EH domains (EH1, EH2, EH3) as well as the full ^{15}N EH123 (200 µM) in the absence and presence of Dab2$_{320\text{-}495}$ at a ^{1}H frequency of 600 MHz. Combined CSPs between the ^{1}H-^{15}N HSQC of the full ^{15}N EH123 domain in the presence of Dab2$_{320\text{-}495}$ and/or Eps15$_{IDR}$ (bottom). **(E)** ^{15}N $R_{1\rho}$ spin relaxation of Dab2$_{320\text{-}495}$ alone (gray, 100 µM) and in the presence of 100 µM EH123 (light blue), and 100 µM of EH123 and Eps15$_{IDR}$ (dark blue) at a ^{1}H frequency of 600 MHz. Below, CSPs are shown that compare Dab2$_{320\text{-}495}$ ^{1}H-^{15}N HSQC spectra in the presence of EH123 with those in the presence of EH123 and Eps15$_{IDR}$. Color legends are displayed in the respective plots.

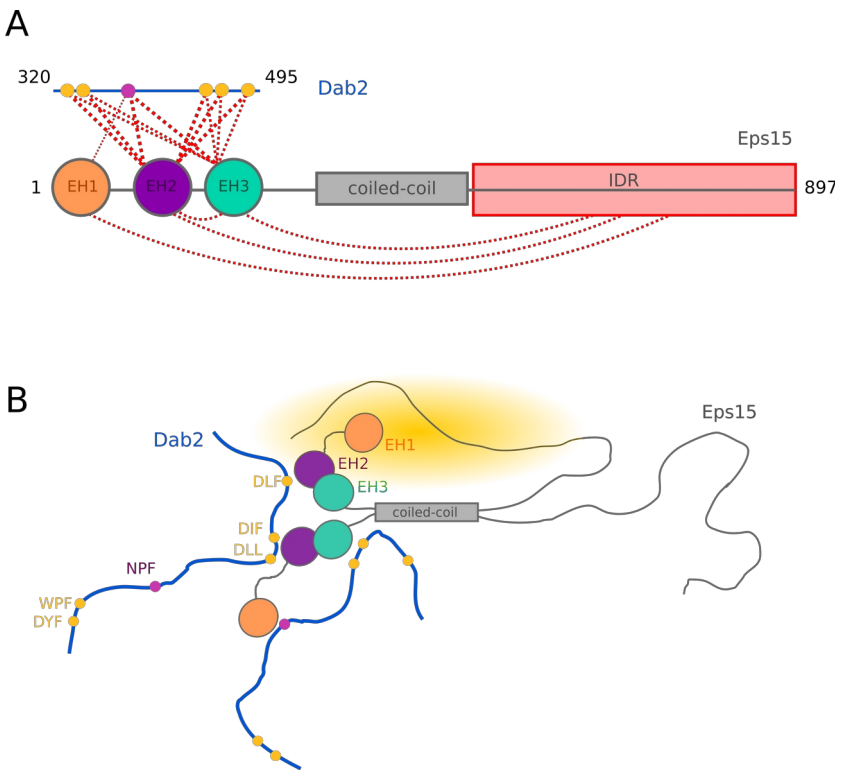

Figure 5. Scheme of Eps15:Dab2 interaction. (A) Visualization of the interaction network of Eps15 and Dab2. On top of Eps15: Inter-molecular interactions between Eps15 and $Dab2_{320\text{-}495}$. Interactions are visualized in red dashed lines. Below Eps15: Intra-molecular interactions within Eps15. Interactions between EH domains and Eps15's IDR were not further localized within the sequence and are thus visualized by a red box. **(B)** Cartoon of self-interactions within Eps15 and between Eps15 and Dab2. Eps15 EH domains interact transiently with Eps15's IDR (illustrated in yellow shading). EH2 and EH3 tumble together. All three EH domains interact with the NPF motif within Dab2, while EH2 and EH3 interact additionally with other motifs along the sequence of $Dab2_{320\text{-}495}$. Dab2 and $Eps15_{IDR}$ interact with EH domains simultaneously and in a dynamic fashion.